Project Title:

Theoretical study of interaction between tunneling electrons and individual molecules at surfaces

Name:
Yousoo Kim, Hyung-Joon Shin, Kenta Motobayashi, Jaehoon Jung

Affiliation:
Surface Chemistry Laboratory, Advanced Science Institute, Wako Institute

---

1. Background and purpose of the project, relationship of the project with other projects.

During the past decade, computer simulations based on a quantum mechanics have developed an increasingly important impact on solid-state physics and chemistry and on materials science. In field of material science, the surface chemistry is fundamentally important to many areas, such as molecular electronics, heterogeneous catalyst, fuel cell, and so forth. The adsorption of molecules on to a surface is a necessary prerequisite to any surface mediated chemical process. Understanding the bonding nature between the molecule and the surface on the basis of the electronic structure is therefore one of the most important issues in this field. The computational methods like density functional theory (DFT) have played a prominent role to elucidate the interaction between the molecule and the surface.

From the theoretical investigation of the adsorbed molecule on surface in combination with STM experiment, we could expect the following research goals; 1) the deep understanding of the chemical/physical properties of an adsorbate on the surface, 2) the fine control of the chemistry on the surface.

2. Specific usage status of the system and calculation method

We have been studying the single molecule adsorption on the well-defined metal surface using computational method in combination with experimental method. In our studies, first-principles simulations have been carried out using the Vienna Ab-initio Simulation Package (VASP) code in the density functional level of theory. The Perdew-Wang exchange-correlation functional has been used and the inner electrons are replaced by projector augmented wave pseudopotentials (PAW). The climbing image nudged elastic band method (CI-NEB) was used to determine the minimum energy paths (MEPs) and the transition states were confirmed by imaginary frequency modes The projected density of states (PDOS) analysis onto the molecular orbital of adsorbate has been performed in order to clarify the distribution of the molecular states near the Fermi level using the first-principles molecular dynamics program, STATE (Simulation Tool for Atom Technology). STM image simulations were performed using Tersoff-Hamann approach. The computational results have been compared with the available experimental result of our group, such as STM and STM-IETS.

Especially, the following researches have been done and have been submitted to the academic international journals. The members registered as the user of RICC system in FY2009 are indicated by

underline.)

(1) State-selective Dissociation of a Single Water Molecule on an Ultrathin MgO Film (H.-J. Shin, J. Jung, K. Motobayashi, S. Yanagisawa, Y. Morikawa, Y. Kim, and M. Kawai)

(2) Controlling Water Dissociation on an Ultrathin MgO Film by Tuning Film Thickness (J. Jung, H.-J. Shin, Y. Kim, and M. Kawai)

(3) Termination and surface species of the magnetite (111) surface studied by scanning tunneling microscopy (T. K. Shimizu, J. Jung, H. S. Kato, Y. Kim, and M. Kawai)

3. Results and Discussion

(1) State-selective Dissociation of a Single Water Molecule on an Ultrathin MgO Film & (2) Controlling Water Dissociation on an Ultrathin MgO Film by Tuning Film Thickness

The interaction of water with oxide surfaces has drawn considerable interest, owing to its application to problems in diverse scientific fields. Atomic-scale insights into water molecules on the oxide surface have long been recognized as essential for fundamental understanding of the molecular processes occurring there. Here, we have performed the STM study of single water molecules on MgO(100)/Ag(100) combined with the first-principles density functional theory (DFT) calculation.

In the STM experiment, the water molecule is adsorbed at atop sites of the Ag(100) surface beneath the 2 ML MgO film, which correspond to Mg^{2+} sites of the MgO surface (Fig. 1).

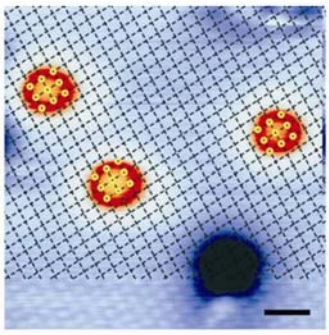

Figure 1. STM image of water molecules on 2 ML thick MgO (V_s = 100 mV and I_t = 0.3 nA). The length of scale bar is 1 nm.

Figure 2 shows the vibrational induced dissociation of water molecule on the 2 ML MgO film. The dissociated products always sit at the bridge site of MgO (Fig. 2b).

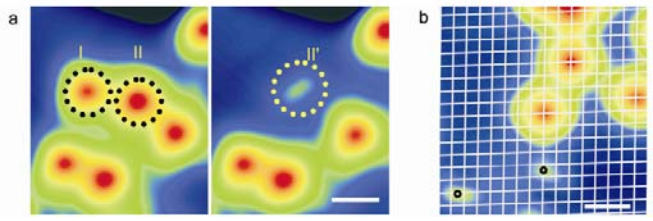

Figure 2. Vibrationally induced dissociation of water molecules. (a) STM images of water molecules before (left) and after (right) applying biases (V_s = 50 mV and I_t = 0.3 nA). Biases of 460 mV with tunnelling currents of 3 nA and 5 nA were applied at I and II independently. (b) STM image of water molecules and dissociated water molecules (V_s = 50 mV and I_t = 0.3 nA). Each point where the lines cross corresponds to a Mg^{2+} ion. The scale bars in (a) and (b) represent 1 nm.

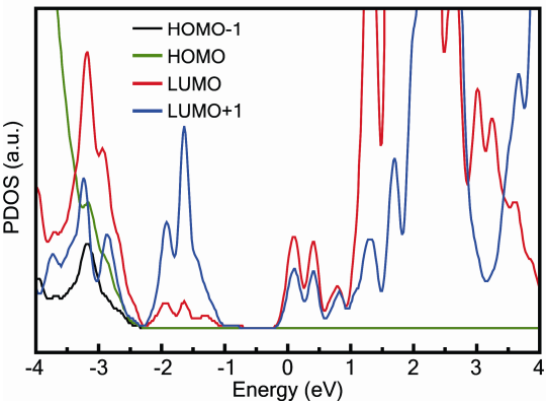

Figure 3. The calculated PDOS of a water molecule on an MgO film. Black, green, red, and blue lines represent HOMO-1, HOMO, LUMO, and LUMO+1, respectively. The zero of energy corresponds to the Fermi energy.

The existence of density of states (DOS) of an adsorbate near the Fermi energy (E_F) is essential for the resonant model of electron-vibration coupling induced by inelastically tunneled electrons (Fig. 3).

Figure 4 shows the structures of adsorbates and the reaction energy for the dissociation of a single water molecule on the MgO(n ML)/Ag(100) (n = 1, 2, and 3) and MgO(100) surfaces. The water molecule first adsorbs asymmetrically on top of the surface magnesium, where one hydrogen atom interacts with a neighboring surface oxygen atom via hydrogen bonding, which is in good agreement with STM image (Fig. 1). In addition, Figure 4 clearly indicates that the chemical activity of the ultrathin MgO film is sensitive to film thickness. This implies that catalytic activity on ultrathin MgO films can be controlled by film thickness.

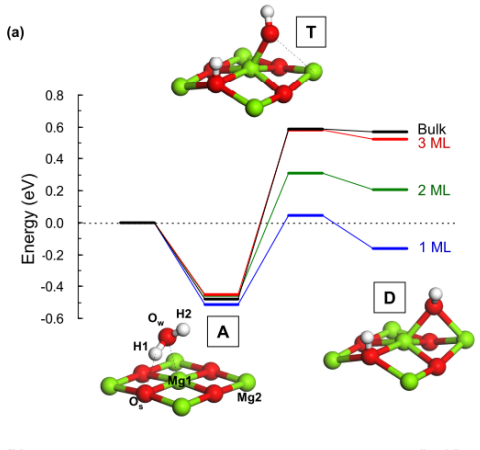

(b) (in eV)

	E(A)	E(T)	E(D)	E_a
MgO(1 ML)/Ag(100)	–0.51	0.05	–0.16	0.56
MgO(2 ML)/Ag(100)	–0.46	0.31	0.21	0.77
MgO(3 ML)/Ag(100)	–0.45	0.58	0.53	1.03
MgO(100)	–0.48	0.59	0.57	1.07

Figure 4. (a) The energy diagram (in eV) for the dissociation of a water single molecule on MgO(n ML)/Ag(100) (n = 1, 2, and 3) and MgO(100) surfaces and the corresponding atomic structures for n = 2 (H, white; O, red; Mg, green). (b) Non-dissociative adsorption (**A**), transition (**T**), and dissociative adsorption (**D**) state energies are evaluated relative to $E(H_2O)$ + E(Substrate) = 0 eV, and the activation energy, E_a is E(**T**) – E(**A**).

On MgO films of 2 ML thickness, the dissociation barrier of water is 770 meV. Therefore, if vibrational excitation is a driving force for the dissociation of water, we expect that the energy of at least two electron processes is required to overcome the dissociation barrier by the excitation of the ν_{OH} mode (448 meV). In addition, the computationally predicted dependence of chemical reactivity on the film thickness is in good agreement with the the experimental observation in which the water molecules on the 3 ML MgO film cannot be dissociated by the vibrational excitation.

The film thickness dependence of chemical reactivity for water dissociation is closely correlated with both the geometric and the electronic natures of the oxide-metal interface because of (1) the large interface distance allowing severe geometric distortion due to water dissociation (Fig. 5) and (2) the strong hybridization of the interface electronic states stabilizing the highly distorted oxide film (Fig. 6).

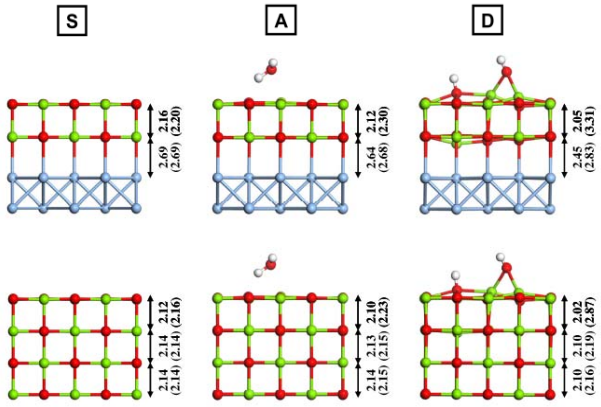

Figure 5. The side views of optimized structures before water adsorption (**S**), in a non-dissociative adsorption state (**A**), and at a dissociative adsorption state (**D**) for the MgO(2 ML)/Ag(100) and MgO(100) surfaces with the minimum (maximum) atomic distances (in Å) of the Mg– or Ag–O bond in the z-direction.

In Fig. 5, before water adsorption (S), the interface distances are considerably larger than other layer-to-layer distances in MgO layers of both the films and the bulk by ~0.5 Å. As a result of the large interface distance, the differences between minimum and maximum interface distances at dissociative

adsorptive adsorption states (D) reach to 0.98 Å and 0.38 Å for the 1- and 2-ML MgO films, respectively.

Figure 6 shows that, after water dissociation (**D**) for the 1-and 2-ML MgO films, the tails of the DOS plots broaden into the higher energy region (red arrow in Fig. 6). This implies that the interaction between electronic states at the oxide-metal interface is increased. This agrees exactly with the previously demonstrated relationship between chemical activity and thickness changes (See Fig. 4). Therefore, the increase of covalent bond strength between the oxide layer and the metal substrate at the oxide-metal interface plays an important role in enhancing the chemical activity on the surface, although the covalent interaction between them is not so strong as tight ionic interaction within oxide layers.

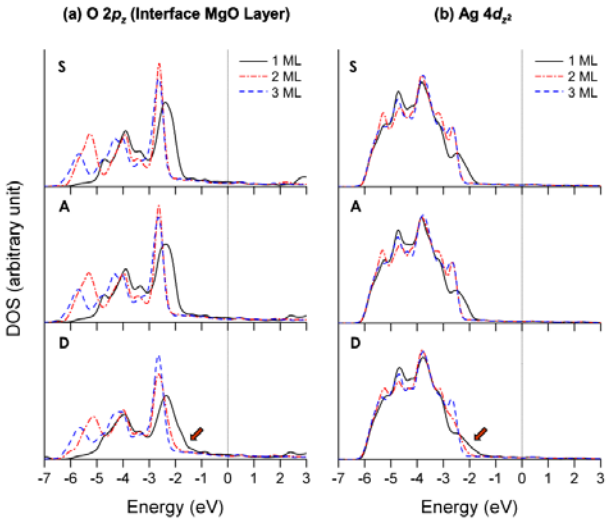

Figure 6. Projected density of states of the *z*-component of (c) Ag 4*d* and (d) O 2*p* states for MgO(*n* ML)/Ag(100) (*n* = 1, 2, and 3) before water adsorption (**S**), at a non-dissociative state (**A**), and at a dissociative adsorption state (**D**). PDOS are plotted for the oxide-metal interface region (MgO 1 L + Ag 2 L) [E_F = 0 eV].

In addition, we could also dissociate water by applying a bias corresponding to the lowest unoccupied molecular orbital (LUMO) energy. When we applied a sample bias voltage of 1.5 V to the water molecule, it splits into dissociated products, as shown in Fig. 7.

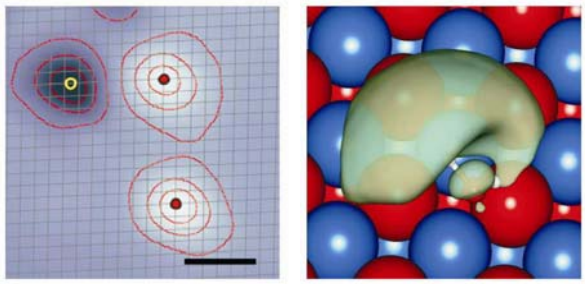

Figure 7. (Left) STM image of water (protrusions) and oxygen (depression) on MgO (V_s = 100 mV and I_t = 0.5 nA). The yellow and red circles indicate the adsorption sites of oxygen and water, respectively. The scale bar represents 1 nm. (Right) Charge density distribution for the LUMO (1.55 eV) of water on MgO.

When tunneling electrons flow directly into the LUMO level of water (Right panel of Fig. 7), the OH bonds are weakened by the occupation of anti-bonding orbitals, leading ultimately to the dissociation of water. The calculated charge density for the LUMO of water shows that nodal planes are located at the OH bonds, which suggests that the LUMO is strongly involved in splitting a water molecule. The adsorption sites of available dissociation products have been also identified using DFT calculations (Fig. 8).

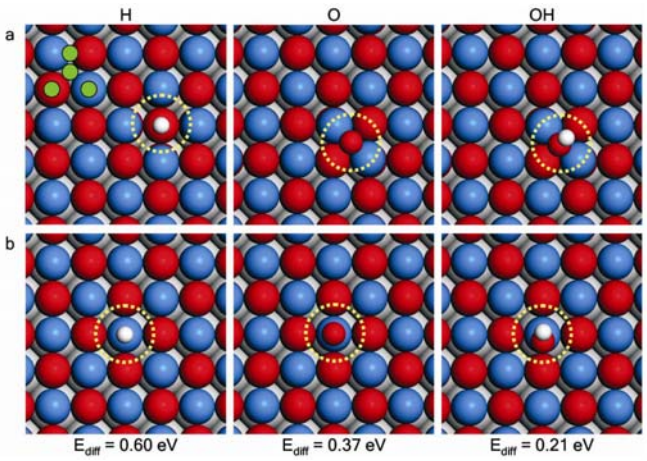

Figure 8. Adsorption configurations of water dissociation products on an MgO film. Results of DFT calculations of (a), the most stable and (b), other equilibrium configurations of hydrogen (left), oxygen (middle), and hydroxyl (right). E_{diff} represents the total system energy difference between (a) and (b) configurations of each species ($E_{b,TOTAL}$ - $E_{a,TOTAL}$). Green circles (upper left corner of a) represent the initial adsorption sites for the calculations.

In summary, two types of dissociation pathways–vibrational excitation and electronic excitation–are selectively achieved by means of injecting tunneling electrons at the single molecule level, resulting in different dissociated products according to the reaction paths (Fig. 9). These two different routes for the controlled dissociation of water molecules using an insulating film as a substrate presents an opportunity that is largely not feasible on metal surfaces. Also, based on our computational results, we propose that the film thickness and the adhesion strength between oxide and metal substrates are key factors in controlling the heterogeneous catalytic activity of an ultrathin oxide film supported by a metal substrate.

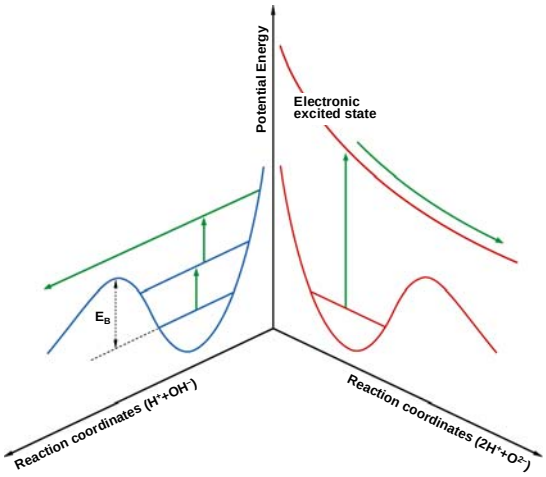

Figure 9. Two types of dissociation pathways for water dissociation.

(3) Termination and surface species of the magnetite (111) surface studied by scanning tunneling microscopy

It is crucial to determine the most energetically stable surface termination because the reactivity of the surface strongly depends on the atomic composition and structure including defects, impurities, and adsorbates that are commonly present on the surface. To confirm the stable termination of $Fe_3O_4(111)$, scanning tunneling microscopy (STM) and spectroscopy (STS) combined with first-principles simulations have been performed.

The (1×1) surface supercells were employed to describe Fe_{tet1} and Fe_{oct2} terminated $Fe_3O_4(111)$ surfaces (Fig. 10(a)). Figure 10(b) shows the slab model used in the calculation, which are periodically separated by about 18 Å.

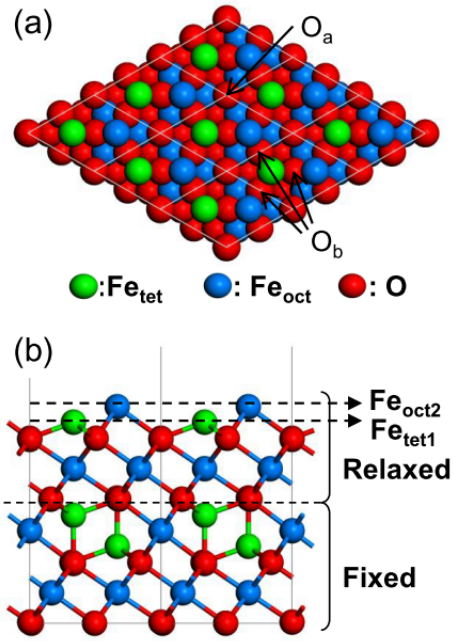

Figure 10. Schematic diagram of atomic arrangement of the $Fe_3O_4(111)$ surface in cubic phase used in the calculations. Top view (a) and side view (b) for the Fe_{oct2} termination are shown. The Fe_{tet1} termination can be constructed just by removing the last Fe_{oct2} layer from the schematics.

In the experiment, when the surface still contained a small portion of oxygen deficient area even after a cleaning cycle using annealing in O_2 atmosphere, we also found another type of surface structure (B) right next to the region of the regular termination (A). Figure 11 shows STM images containing such an area. Region A corresponds to the regular termination. It appeared as a hexagonal lattice with any bias voltage in any tip condition. New region marked as B, on the other hand, appears either as a honeycomb structure (Fig. 11(a) and 11(c)) or as a hexagonal lattice (Fig. 11(b) and 11(d)) depending on the bias (comparison of (a) and (b)) and tip condition (comparison of (c) and (d)). Sites of protrusions in the

region A are found to correspond to three of six protrusions forming the honeycomb structure in the region B (Fig. 11(a)), but does not correspond to the sites of protrusions of the hexagonal lattice in B (Fig. 11(b)).

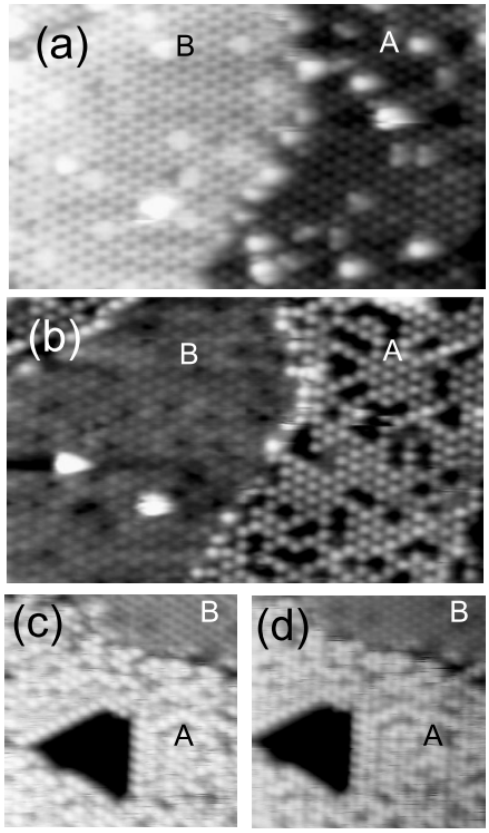

Figure 11. STM images ((a) and (b) 9 nm × 15 nm; (c) and (d) 10 nm × 10 nm) showing bias and tip dependence of the appearances of two regions. Region A corresponds to the regular termination. Appearance of the region B, either honeycomb or hexagonal lattice, depends both on the bias ((a) and (b)) and on the tip condition ((c) and (d)). Tunneling parameters: (a)V_{bias} = +2.0 V and I_t= 0.2 nA; (b) V_{bias}= –2.0 V and I_t= 0.2 nA; (c) and (d) V_{bias}= –1.0 V and I_t= 0.2 nA.

To verify experimental STM images, we performed STM simulations of surfaces terminated by the Fe_{tet1} and Fe_{oct2} layers. Figure 12 shows the results of the bias voltage ±2 V. For the Fe_{tet1} termination, protrusions at the Fe_{tet1} sites (marked by blue triangles) form hexagonal lattice at both bias voltages. In contrast, for the Fe_{oct2} termination, the Fe_{oct2} sites (red circles) appear bright, forming hexagonal lattice at +2 V, whereas both Fe sites are bright resulting in a honeycomb structure at –2 V. These results qualitatively agree well with the experimental observation, but only under certain tip conditions (e.g., the tip taking Fig. 11(c)). The simple Tersoff-Hamann approach generates STM images using the local density of states (LDOS) of surface. However, because the Tersoff-Hamann approach does not include the tip information such as the chemical composition and the geometry, it is not surprising that the bias dependence is different (sometimes opposite) to the real STM images (e.g., Figs. 11(a), 11(b) and 11(d)). The tip that produces different bias dependence from the simulation often yields clearer and sharper images, which is an implication of the chemical modification of the tip apex. Thus it is reasonable that the bias dependence is not completely reproduced by the simulation.

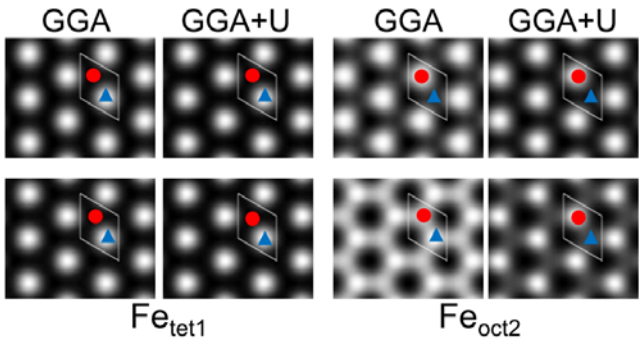

Figure 12. Simulated constant height STM images using GGA and GGA+*U* (*U*= 5 V and *J*= 1V) methods. Four images on the left correspond to Fe_{tet1} termination and four images on the right correspond to Fe_{oct2} termination. Sample bias voltages are set to +2V (upper row) and –2V (lower row). Rhombus in each image corresponds to the unit cell. Blue triangle and red circle indicate the Fe_{tet1} and Fe_{oct2} sites, respectively.

Therefore, we have concluded that the regular surface is terminated by a layer of Fe_{tet1} whereas Fe_{oct2} termination appears only in oxygen poor conditions by combined study of STM and first-principles simulations.

4. Conclusion

We have tried to examine the behaviors of single molecules on the metal supported insulating metal oxide surface and the regular termination of transition metal oxide surface using the first principles calculations. First, the vibrational excited dissociation of water molecule on the ultrathin MgO film supported Ag substrate has been successfully explained. Based on the computational results, we have proposed the two factors – the well-defined film thickness and the adhesion energy between oxide film and metal substrate – to design heterogeneous catalyst for water dissociation using a metal-supported oxide film. Second, the regular termination of $Fe_3O_4(111)$ has been confirmed by the STM simulation using the Tersoff-Hanmann method. Our computational study combined with STM experiment shows the benefits of the computational approach to clarify the experimental results and to give a light for further experiments, especially, at the single molecule regime on the surface and at the surface structure verifications.

5. Schedule and prospect for the future

The following research topics are being (or will be) performed till September, FY2010 on RICC system.

(1) The effect of interface defects on the chemical reactivity for water dissociation on the oxide film supported by metal substrate. (J. Jung, H.-J. Shin, and Y. Kim)
(2) CO hopping induced by surface phonon on the ultrathin oxide film (H.-J. Shin, K. Motobayashi, and Y. Kim)
(3) Lowest Unoccupied Molecule Orbital (LUMO) mediated interaction between organic aromatic molecule and metal surface (J.-H. Kim, H.-J. Shin, and Y. Kim)
(4) STM image simulation of fluorofullerene on Au(111) surface (T. Otani, J. Jung, and Y. Kim)
(5) The remote control of chemical activity by dopants or impurities at the interface of metal supported oxide film surface. (H.-J. Shin, J. Jung, and Y. Kim)

6. If you have a "General User" account and could not complete your allocated computation time, specify the reason.

Our account status is a "General User" as a Group user (Group leader: Yousoo Kim). In addition, the period of our project using RICC system is ~ September 30th, 2010. Until now, we have used 13.6 % of the assigned CPU resources to us.

7. If no research achievement was made, specify the reason.

2 papers are currently in revision (*Nature Materials* and *Physical Review B*), and 1 paper has been submitted (*Physical Review B*).

Fiscal Year 2009 List of Publications Resulting from the Use of RICC

* The members registered as the user of RICC system in FY2009 are indicated by underline.

[Publication]

- H.-J. Shin, J. Jung, K. Motobayashi, S. Yanagisawa, Y. Morikawa, Y. Kim, and M. Kawai, "State-selective Dissociation of a Single Water Molecule on an Ultrathin MgO Film", *Nat. Mater.*, in revision.

- J. Jung, H.-J. Shin, Y. Kim, and M. Kawai, "Controlling Water Dissociation on an Ultrathin MgO Film by Tuning Film Thickness", *Phys. Rev. B*, in revision.

- T. K. Shimizu, J. Jung, H. S. Kato, Y. Kim, and M. Kawai, "Termination and surface species of the magnetite (111) surface studied by scanning tunneling microscopy", *Phys. Rev. B*, submitted.

[Oral presentation at an international symposium]

- Y. Kim, "Electronic Structure of a Carbon nanotube on Various Electrode Surfaces", ISSP workshop on physics and new phenomena of π-electronic interfaces", Aug. 10-12, 2009, Chiba, Japan.

- Y. Kim, "Action spectroscopy for vibrationally induced motion and reaction of single molecules", ECOSS26, Aug. 30-, 2009, Parma, Italy.

- Y. Kim, T. Okada, and M. Kawai, "State-resolved study of surface dynamic processes of a single molecule by scanning tunneling microscopy", ICESS11, Oct. 10, 2009, Nara, Japan.

- T. K. Shimizu, Y. Kim, and M. Kawai, "Termination and identification of surface species of the magnetite (111) surface studied by scanning tunneling microscopy", American Vacuum Society 56th International Symposium and Exhibition, Nov. 8-13, 2009, San Jose, CA.

- H.-J. Shin, J. Jung, K. Motobayashi, Y. Kim, and M. Kawai, "Isolated Single Water Molecules on Ultrathin MgO Film Studied by Scanning Tunneling Microscope", American Vacuum Society 56th International Symposium and Exhibition, Nov. 8-13, 2009, San Jose, CA.

- Y. Kim, "Single Molecule Chemistry; When a Molecule Meets Electrons", RIKEN Asian Research Network Symposium "Toward Fusion Nanotechnology", Feb. 17, 2010, Tokyo, Japan.